JARS Journal of Applied Remote Sensing

RESEARCH PAPER

# Use of unmanned aerial vehicle-derived multi-spectral data for the early detection of multi-temporal maize leaf equivalent water thickness and fuel moisture content for the improved resilience of smallholder maize farming

**Helen S. Ndlovu**,[a,*] **John Odindi**,[a] **Mbulisi Sibanda**,[b] **Onisimo Mutanga**,[a] **Alistair Clulow**,[c] **Vimbayi G. P. Chimonyo**,[d,e] **and Tafadzwanashe Mabhaudhi**[d]

[a]University of KwaZulu-Natal, School of Agricultural Earth and Environmental Sciences, Discipline of Geography and Environmental Science, Pietermaritzburg, South Africa

[b]University of the Western Cape, Department of Geography, Environmental Studies and Tourism, Faculty of Arts, Cape Town, South Africa

[c]University of KwaZulu-Natal, Discipline of Agrometeorology, School of Agricultural, Earth and Environmental Sciences, Pietermaritzburg, South Africa

[d]University of KwaZulu-Natal, School of Agricultural, Earth and Environmental Sciences, Centre for Transformative Agricultural and Food Systems, Pietermaritzburg, South Africa

[e]International Maize and Wheat Improvement Center-Zimbabwe, Mt. Pleasant, Harare, Zimbabwe

**ABSTRACT.** Maize water stress from rainfall variability is a key challenge in producing rain-fed maize farming, especially in water-scarce regions, such as southern Africa. Hence, quantifying maize foliar water content variations throughout the phenological stages is valuable in detecting smallholder maize moisture stress and supporting agricultural decision-making. The emergence of unmanned aerial vehicles (UAVs) equipped with multispectral sensors offers a unique opportunity for robust and rapid monitoring of maize foliar water content and stress. The combination of near-real-time spatially explicit information acquired using UAV imagery with physiological indicators, such as equivalent water thickness (EWT) and fuel moisture content (FMC), provides viable options for detecting and quantifying maize foliar water content and moisture stress in smallholder farming systems. Therefore, we evaluated the utility of UAV-based multispectral datasets and random forest regression in quantifying maize EWT and FMC throughout the maize phenological growth cycle. Results showed that EWT and FMC could be determined using the near-infrared and red-edge wavelengths to a relative root mean square error of 2.27% and 1%, respectively. Specifically, the spectra acquired during the early reproductive growth stages between silking and milk stages demonstrated a high sensitivity to the variation in maize moisture content. These findings serve as a fundamental step toward creating an early maize moisture stress detection and warning system and contribute to climate change adaptation and resilience of smallholder maize farming.

 [DOI: 10.1117/1.JRS.18.014520]

**Keywords:** maize moisture; phenology; growing season; spatio-temporal variability; precision farming

Paper 230679G received Dec. 12, 2023; revised Jan. 18, 2024; accepted Feb. 16, 2024; published Mar. 8, 2024.

*Address all correspondence to Helen S. Ndlovu, 216016417@stu.ukzn.ac.za

1931-3195/2024/$28.00 © 2024 SPIE

## 1 Introduction

Maize (*Zea mays L.*) is an important and eminent food security crop that also serves as a valuable source of animal fodder, bio-energy, and raw industrial material.[1,2] However, due to rainfall scarcity and variability, maize moisture stress is a serious abiotic threat to maize production.[1,3] Subsequently, water deficit negatively impacts maize productivity and impairs crop growth and development, significantly reducing yield.[1,4] Sah et al.[2] reported that yield loss could vary from 30% to 90% depending on the crop stage and the degree and duration of water deficit stress. The stages of maize susceptible to water deficit stress are the vegetative, silking (flowering), and early stages (grain filling),[4] where yield loss may be as high as 25%, 50%, and 21%, respectively.[2] The most obvious cause of yield losses as a result of water deficit stress is the loss of or suppressed phenotypic expression and could manifest as a reduction in the canopy size, green-leaf duration, plant height, leaf number, early leaf senescence, and asynchronized flowering.[1,2,4] However, before many of these phenotypic responses are expressed, water deficit would have caused irreversible damage to crop physiological processes.[5] Early detection of physiological damage or disruption can be key to developing adaptive strategies for increasing smallholder maize resilience to water stress.

The most widely used physiological indicators of maize foliar moisture content are equivalent water thickness (EWT) and fuel moisture content (FMC).[3,6–8] EWT is a leaf water status metric defined as the ratio between the quantity of water and leaf area.[8] Zhang and Zhou[9] noted that EWT is closely associated with plant biochemical processes, such as photosynthesis, plant metabolism, and crop evapotranspiration; hence it is a suitable indicator of moisture stress. FMC is defined as the proportion of water to dry matter[7] and has been widely used for plant water stress, drought monitoring, and as a measure of ignition and fire propagation potential.[3,7,10] Studies by Ndlovu et al.[3] and Zhang and Zhou[9] demonstrated the performance of EWT and FMC as valuable indicators of the maize water content in smallholder farming systems. Therefore, quantifying maize leaf EWT and FMC can provide valuable information for the early detection of maize moisture stress and monitoring of maize physiology throughout the growth period to inform small-scale agricultural decision-making.

Conventionally, maize EWT and FMC variations rely on direct measurements and the visual assessment of maize physiology conducted by trained experts.[11] However, these methods are extremely time-consuming, tedious, subject to human error, and cannot sufficiently reflect spatial and temporal variability in maize moisture status.[6,12,13] Furthermore, field data collection requires continuous measurements throughout the maize growth cycle, making implementation marginally feasible.[11,14] Consequently, there is a need for methods that can provide spatially explicit datasets with a high temporal ability to monitor changes in smallholder maize leaf moisture content throughout the growth period.

Recent advances in technology, particularly unmanned aerial vehicles (UAVs), have heralded a new era in remote sensing, mapping, and data analytics within precision agriculture.[15–20] Using lightweight multispectral sensors mounted on UAVs offers great possibilities for continuous near-real-time crop monitoring at a farm level.[11] UAVs are unique because they can provide high-quality remotely sensed data at unprecedented spatial, spectral, and temporal resolutions.[3,15] In addition, UAVs mounted with sensors capture imagery at low altitudes. They can hover over areas of interest, making them a desirable tool for monitoring changes in maize moisture content at different phenological stages.[21]

Furthermore, UAVs provide a cost-effective option to obtain frequent imagery at an ultra-high spatial resolution, often in centimeters, which is necessary for monitoring crop physiology at a plot level.[18,20,22] For example, in a comparative study between UAV-based data and satellite imagery, Matese et al.[23] confirmed that UAV-derived datasets can detect even the most subtle variations in crop physiological characteristics, a challenge even for high-resolution satellite imagery such as RapidEye. A study by Tang et al.[17] demonstrated the value of UAV-derived multispectral data in predicting maize evapotranspiration with an $R^2$ of 0.81 and RMSE of 0.95 mm/day. Nonetheless, the ability of UAV imagery to adequately discriminate maize foliar moisture content variability across the growing stages remains untested. Therefore, the potential application of UAVs equipped with multispectral sensors in characterizing smallholder maize moisture status at different growth stages still requires investigation.

Since the moisture content in leaf tissue is a critical determinant of crop survival, accurately monitoring crop water status using spectral reflectance measurements has been a key objective in environmental research.[24] The rationality of estimating maize moisture content stems from the fact that literature confirms the existence of a strong relationship between foliar water concentration and spectral absorption at specific near-infrared (NIR) and the shortwave infrared wavelengths of the electromagnetic spectrum.[25] For instance, water molecules in leaf tissue produce maximum absorption features along the NIR (750 to 1300 nm) section of the spectrum due to a decrease in leaf reflectance.[24,26,27] Furthermore, there are secondary effects of water absorption in the visible region of the electromagnetic spectrum (blue, green, and red) which are influenced by internal leaf structure and water transmissivity.[6,25] This makes these sections of the spectrum sensitive to changes in water content and, therefore, a plausible proxy for crop water stress detection. To enhance the spectral characteristics of crop leaf reflectance, several studies have demonstrated the utilization of empirical models and vegetation indices (VIs) to predict crop moisture content.[24,28] For example, studies have reported that the normalized difference water index (NDWI) is a water content-sensitive index that can be used to predict crop moisture throughout the growth stages.[29–32] Krishna et al. [27] noted that even though the normalized difference vegetation index (NDVI) is optimal for crop chlorophyll content estimations, the index is highly correlated to the plant water status; hence it is also a valuable predictor of maize moisture content. Therefore, with the understanding of crop leaf reflectance across the electromagnetic spectrum, UAV-derived spectral datasets provide a viable approach to quantifying intra-species moisture content variability of smallholder maize crops throughout the growth cycle.

The use of machine learning algorithms, such as the random forest (RF), support vector machines (SVM), and multiple linear regression, has have been proven to be instrumental in characterizing crop characteristics.[33] RF has proven to be a valuable regression model and is known for its efficiency in handling outliers, its ability to account for non-linear relationships between multiple variables, and its capacity to produce credible results, even with a small dataset, as was the case in this study.[34,35] The RF algorithm has high computational efficiency in processing non-parametric and high dimensional data while being sensitive to overfitting.[35–37] The success of the RF regression model has been well-documented in recent literature.[38,39] A comparative study by Lee et al.[40] assessed the performance of SVM, multiple linear regressions, and RF algorithms in predicting the canopy nitrogen content of maize. It concluded that the RF yielded the highest prediction accuracies. Again, Shao et al.[37] also found the RF model to outperform traditional regression techniques in estimating the biophysical characteristics of wheat crops. In a similar study, Ndlovu et al.[3] evaluated the performance of five machine learning techniques, namely RF, SVM, decision trees, artificial neural networks, and partial least squares regression, in estimating maize EWT and FMC of smallholder farming systems. In that study, it was established that the RF algorithm outperformed all the other algorithms in optimally predicting maize leaf moisture content parameters.

Considering that limited studies have evaluated the feasibility of using UAV-based proximal remotely sensed data in accurately monitoring maize foliar moisture content across all phenological stages,[9] there is a need to assess the value of UAV-derived data in mapping crop moisture content variability. This study, therefore, sought to evaluate the utility of UAV-derived multispectral imagery in estimating the spatio-temporal variability of smallholder maize leaf EWT and FMC across the maize growing stages.

## 2 Materials and Methods

### 2.1 Study Site Description

This study was conducted in Swayimane (29.51667°S, 30.68333°E), uMshwati Municipality, KwaZulu-Natal, South Africa (Fig. 1). The study area has a sub-tropical climate, with an average annual rainfall between 600 and 1200 mm and an average air temperature between 12°C and 24°C.[41] Swayimane is located at 886 m above sea level and has a relatively flat topography. The soil in the area is classified as deep and dark clay loam soils, which indicates high organic matter and soil fertility. The land in Swayimane is predominantly used for commercial and small-scale subsistence agriculture, with the cultivation of several crops, including taro, sweet potatoes, spinach, beans, sugarcane, and maize. The area is situated within the moist midlands mist belt

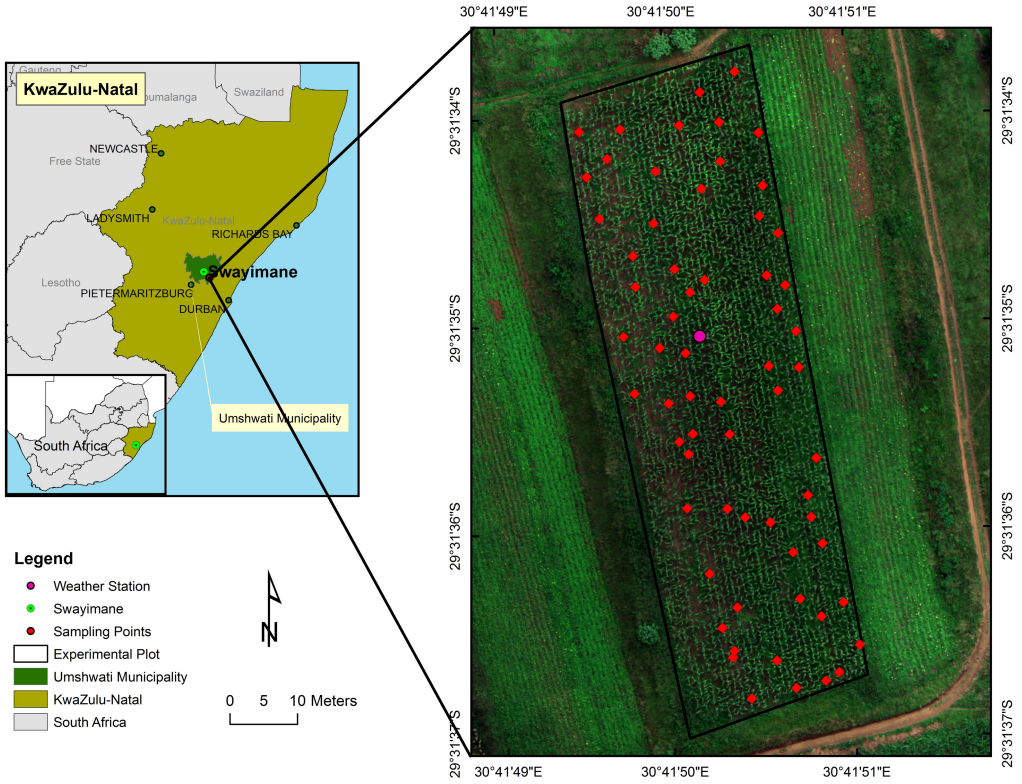


**Fig. 1** Location of the study area in Swayimane, South Africa.

bioclimatic region prone to berg winds, extreme clouds, flash floods, seasonal hail, and occasional drought. The area has been identified as a climate change hot spot.[42] Climate projections of the area indicate an increase in temperature and unpredictable variations in annual precipitation resulting in an increased risk of climate-driven events, including an increase in drought.

### 2.2 Experimental Plot and Crop Management Description

Figure 2 shows the biophysical condition of maize at the various phenological growth stages. (Description of growth stages is available in Table 1.) The experimental plot was 50 m long and 30 m wide and was located on a gentle slope. Maize crops were sown on February 8, 2021, and corn kernels were harvested on May 17, 2021. Cow urea and manure were manually spread in the experimental field before sowing as a source of nutrients to fertilize the soil. A combination of manual hand weeding and herbicide application was conducted when the maize crops were 21 days old. The experimental plot relied primarily on precipitation as a source of water supply. The study plots were not irrigated nor applied fertilizer during the growing season. Table 2 presents the bioclimatic conditions of the study plot during the maize growing period, derived from an automatic weather station located ~860 m from the experimental plot.

### 2.3 Field Survey and Measurements of Maize Moisture Content

Field measurements were conducted on March 18 (V8-V10), March 31 (V14-Vt), April 12 (R1-R2), April 28 (R2-R3), and May 14 (R3-R4) in 2021. Prior to the field survey, the boundary of the experimental plot was digitized in the Google Earth Pro domain. The digitized polygon was imported into ArcGIS and used to generate sampling points. A stratified random sampling procedure was used to generate 65 random sampling points within the experimental plot.[43] This method is optimal for acquiring an unbiased representative sample of the experimental maize plot.[43,44] A Trimble handheld GPS with a sub-meter accuracy was used to navigate to these sampling points at each stage of the maize growth period. The third fully developed maize leaf from the top of the stalk was sampled at each sample point. Literature states that to obtain reliable maize physiological measurements, fully developed leaf samples should be taken from the top of the canopy as there is maximum reflectance of light energy.[45,46]

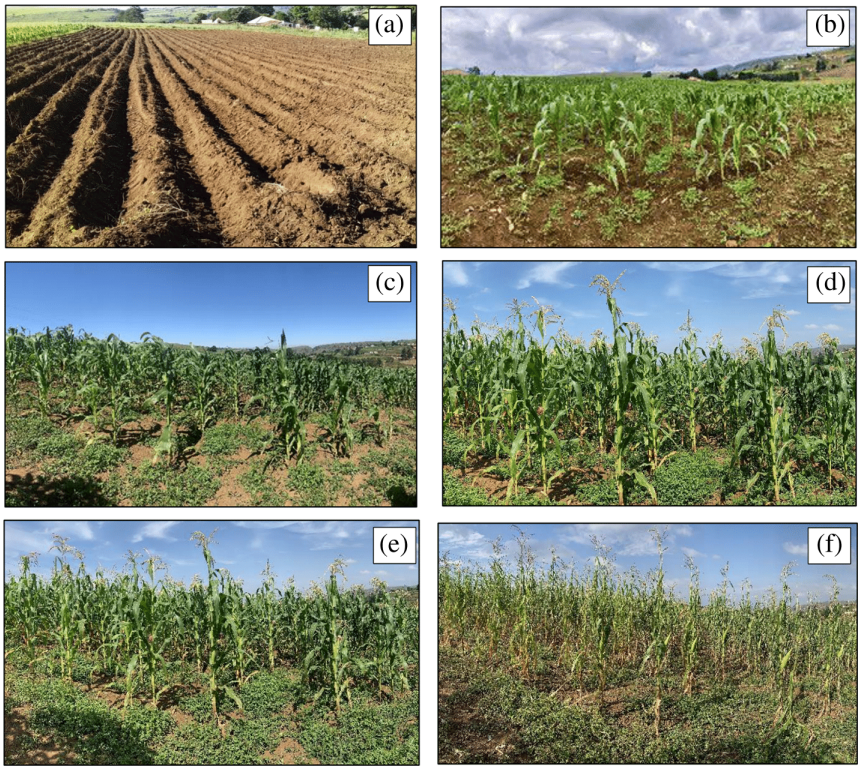


**Fig. 2** Field and maize crop conditions at (a) Pre-sowing, (b) V8–V10, (c) V14–Vt, (d) R1–R2, (e) R2–R3, and (f) R3–R4 of the growth stages.

**Table 1** Description of maize growth stages.

| Growth stage | Description |
|---|---|
| V8–V10 | Maize crop is in the mid-vegetation stage of ear initiation and early cob development |
| V14–Vt | Tassel at growth point begins to develop rapidly until visible |
| R1–R2 | Early reproductive stages where silks are developing. These growth stages exhibit high sensitivity to water deficit |
| R2–R3 | Kernel development |
| R3–R4 | Grain filling. Nutrients are transported to cob |

**Table 2** Bioclimatic condition of maize across the phenological growth period.

| Bioclimatic variable | V8–V10 | V14–Vt | R1–R2 | R2–R3 | R3–R4 |
|---|---|---|---|---|---|
| Total rainfall (mm) | 2.4 | 0.8 | 0 | 0 | 0 |
| Minimum air temperature (°C) | 17.19 | 15.08 | 19.74 | 15 | 12.62 |
| Maximum air temperature (°C) | 23.77 | 22.8 | 31.91 | 30.52 | 27.32 |
| Maximum wind speed (m/s) | 3.76 | 5.09 | 4.07 | 4.14 | 3.76 |
| Total solar irradiance | 1040 | 1043 | 734.1 | 767.9 | 643.2 |
| Maximum atmospheric pressure (mbar) | 918 | 922 | 926 | 921 | 1012 |
| Minimum relative humidity (%) | 67.77 | 67.13 | 28.95 | 16 | 32.93 |

Meanwhile, sampling young crops can lead to plant stress, which can ultimately cease crop growth.[45,47] In this regard, maize leaf sampling was not conducted during the emergence stages, specifically from germination to the fifth leaf collar growth stage. Crop moisture content measurements were conducted under near-cloud-free conditions between 12:00 noon and 14:00 as this is the most optimal photosynthetic period of the day with radiation at maximum.[48] A portable leaf area meter (LI-3000C) with 1 $mm^2$ resolution was used to measure the leaf area ($A$) of sampled leaves. A calibrated scale was used to obtain the fresh weight (FW) of maize leaf samples, which were then dried in an oven at 70°C until a constant dry weight (DW) was reached ($\pm$48 h). The leaf equivalent water thickness ($EWT_{leaf}$ in $gm^{-2}$) and fuel moisture content ($FMC_{leaf}$ in %) were then computed using the FW, DW, and $A$ of maize leaves based on the equation:

$$\mathrm{EWTleaf} = \frac{\mathrm{FW} - \mathrm{DW}}{A}\ \mathrm{Units}: \mathrm{gm}^{-2}, \tag{1}$$

$$\mathrm{FMCleaf} = \frac{\mathrm{FW} - \mathrm{DW}}{\mathrm{DW}} \times 100\ \mathrm{Units}: \%, \tag{2}$$

where FW is the fresh weight, DW is the dry weight, and $A$ is the leaf area. The computed $EWT_{leaf}$ and $FMC_{leaf}$ were recorded in an excel spreadsheet against the coordinate of each sampling point, which was later converted into a point map in ArcMap version 10.3.1. It must be noted that at the beginning of the growing season, we only targeted fully developed and expanded leaves where the leaf collar was visible. That created a bit of randomness in the sampling. Significant deviations from the sampled plants occurred after the area experienced a hailstorm, on April 23, 2021, which damaged maize leaves. As a result, we sampled other maize plants that still had intact leaves. Sampling the undamaged maize plants resulted in different sampling points in the plot at different stages.

### 2.4 UAV Platform, Imagery Acquisition, and Processing

The Altum MicaSense multispectral camera mounted on a DJI Matrice 300 series UAV platform was used to obtain images of the study site at the five phenological growth stages (Fig. 3). The main advantage of this UAV platform is its ability to acquire imagery over a range of environmental conditions at high speed (one image captured per second) and to provide imagery with high geolocational accuracy. The UAV platform is equipped with a downwelling light sensor (DLS 2), which improves the reflectance calibration and the georeferencing of the images. The MicaSense sensor consists of six spectral bands that capture spectral reflectance in the blue (475 nm), green (560 nm), red (668 nm), red-edge (717 nm), NIR (840 nm), and thermal (8–14 nm) regions of the electromagnetic spectrum[3] [Fig. 3(b)]. The boundary of the experimental plot was generated around the plot in the Google Earth Pro domain, as described in Sec. 2.3. The polygon was imported into the UAV's handheld console as a Keyhole Markup Language file format to generate the navigation flight plan. The flight was then carried out by a certified remote pilot at a flight height of 100 m, a ground sampling distance of 9.6 cm (81 cm for the thermal camera), and an 80% image overlap.

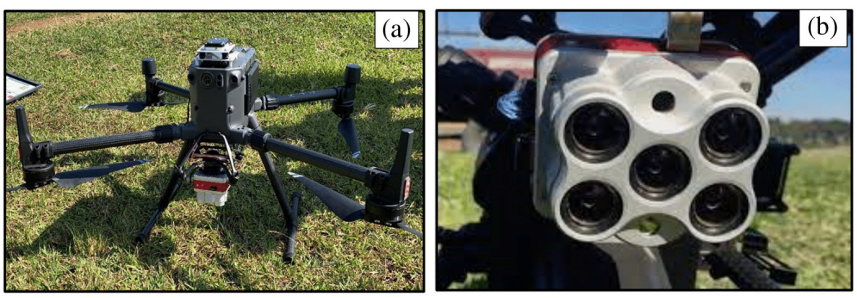


**Fig. 3** (a) UAV imaging platform and (b) MicaSense multispectral camera used in this study.

Before and after each drone flight, the MicaSense camera was calibrated using the MicaSense Altum calibrated reflectance panel. This was conducted by acquiring an image of the calibration panel at ambient atmospheric and solar radiation conditions. These images were imported along with the other captured images used into Pix4D Fields photogrammetry software (Pix4 Fields) for pre-processing. Thereafter, radiometric corrections were conducted on the captured images using both the before and after flight images of the calibration panel. The calibration panel has a white balance card with reflectance properties across the electromagnetic spectrum and was used as the target for the radiometric calibration of the images. This allows the Pix4D software to correct the reflectance of the images to account for the dominant atmospheric conditions at the time of image acquisition.[41]

The raw multispectral data, consisting of ~3400 images per flight, were mosaicked to form a single image of the study area using Pix4D Fields. Pix4D Fields were then used in conjunction with the calibration images based on the map function to calculate reflectance as described in Ref. 49. A total of five ground control points were acquired, one at each corner of the experimental plot and a point at the location of the weather station situated at the center of the maize field. The image was thereafter georeferenced in QGIS 3.4.0 to optimize geolocation accuracy using the five ground control points to an RMSE less than half a pixel (3 cm).

### 2.5 Selection of Vegetation Indices

The six pre-processed spectral bands, acquired using the Mica sense's six spectral channels, were used to estimate maize $EWT_{leaf}$ and $FMC_{leaf}$ These bands were also used to compute VIs used to estimate maize moisture indicators in a GIS environment. Studies have confirmed the ability of VIs computed from the combination of the visible and NIR channels of the electromagnetic spectrum to detect subtle variations in vegetation water characteristics.[24,25] Based on existing literature, 10 moisture content-related VIs were computed based on their correlation with maize moisture content indicators. Table 3 illustrates the equations used to compute VI for estimating maize moisture content. After computing the VIs, the sampling points were overlaid with all the spectral variables (spectral bands and VIs) to extract the spectral signatures used for the statistical analysis.

### 2.6 Model Development and Statistical Analysis

Regression models provide a reliable and efficient method for performing complex and multi-dimensional environmental data analysis that would naturally be time-consuming to observe.[57] In this study, the RF regression algorithm was used to predict maize leaf moisture content indicators ($EWT_{leaf}$ and $FMC_{leaf}$) at different phenological growth stages of maize crops because of its simplicity and robustness.[10]

The RF ensemble is a machine-learning technique that uses bootstrap aggregation and binary recursive partitioning to construct several independent trees using a random subset derived

**Table 3** Selected VIs used for maize moisture content estimations.

| Vegetation index | Equation | References |
|---|---|---|
| NDWI | (Green − NIR/green + NIR) | 50 |
| NDVI | (NIR − red/NIR + red) | 51 |
| NGRDI | (Green − red/green + red) | 52 |
| NDRE | (NIR − rededge/NIR + rededge) | 53 |
| $NDVI_{rededge}$ | (Rededge − red/rededge + red) | 53 |
| $CI_{green}$ | ((NIR/green) −1) | 54 |
| $CI_{rededge}$ | ((NIR/rededge) −1) | 9 |
| SR | (NIR/red) | 55 |
| OSAVI | [(NIR − red)/ (NIR + red + 0.16)] × (1 + 0.16) | 56 |

from the training data.[57] The robustness of RF originates from the capacity of the algorithm to use bootstrap aggregation to build regression trees that are grown to their maximum sizes, which are then used to allocate an input variable (spectral bands and VIs) to a response variable ($EWT_{leaf}$ or $FMC_{leaf}$) using unweighted averaging.[58] In addition, the out-of-bag samples, which have been excluded from the bootstrap aggregation, are used by the RF ensemble to evaluate the generated regression model.[59] However, a common challenge with regression models is multicollinearity which results from a high level of correlation between two or more predictor variables.[60] Using only the most suitable predictor variables in building regression models[56] is advisable. Variable importance selection was adopted to resolve potential collinearity and select the best and the fewest predictor variables for the RF model. RF can compute Gini impurity scores used to identify predictor variables most influential in prediction.[10] Therefore, a high Gini impurity score identifies the most important predictor variable. The best predictor variables were then used to develop the final RF model of maize moisture content at each growth stage. Subsequently, RF was used in this study because of its ability to identify and select optimal predictor spectral features while circumventing inherent autocorrelations.[61,62] Furthermore, it has a bootstrap mechanism that makes it applicable regardless of the sample sizes and does not require any data assumptions.[63] The optimal hyperparameter values for the prediction of maize water content in the study was determined to be an *Ntree* equal to 500 and an *Mtry* of 11 after numerous iterations.

Before the analysis, the data were randomly split into training data (70%) and validation data (30%). The former was used to develop the regression model, and the latter to evaluate the model's predictive performance. In developing the UAV remotely sensed-based $EWT_{leaf}$ or $FMC_{leaf}$ models, the relative performance of spectral bands was evaluated to that of VIs. Subsequently, the combined optimal prediction bands and VIs were used to model the spatial variability of $EWT_{leaf}$ or $FMC_{leaf}$ across different phenological stages of maize crops.

### 2.7 Model Validation

The prediction accuracy of the derived RF models was assessed based on the coefficient of determination ($R^2$), the root mean square error (RMSE), and the relative root mean square error (rRMSE). The optimal model for estimating maize moisture content indicators at different phenological stages was determined based on the highest $R^2$ and the lowest RMSE and rRMSE:

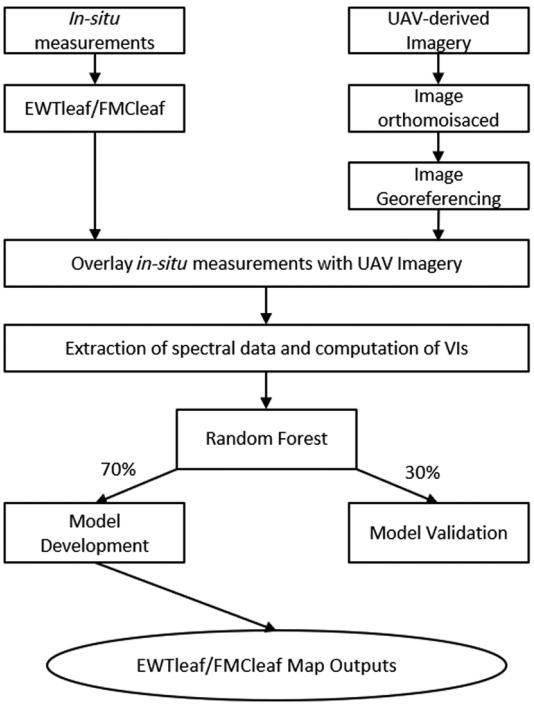


**Fig. 4** Flowchart of methodology implemented in this study.

$$\mathrm{RMSE} = \sqrt{\frac{\sum(\text{predicted} - \text{actual})^2}{n}}, \tag{3}$$

$$\mathrm{rRMSE} = \frac{\mathrm{RMSE}}{\mathrm{Mean(actual)}} \times 100, \tag{4}$$

where predicted is the modeled variable and actual is the field-measured variable. Lastly, a map illustrating the spatial and temporal distribution of the predicted maize $EWT_{leaf}$ or $FMC_{leaf}$ at every growth stage was generated using the optimal predictor variable derived from the optimal regression model on ArcMap version 10.3.1 software. The RMSE and the rRMSE were calculated based on the above equations. A systematic flow diagram of the methodology implemented in this study is presented in Fig. 4.

## 3 Results

### 3.1 Estimating Maize $EWT_{leaf}$ and $FMC_{leaf}$ Throughout the Maize Growing Stages

In general, UAV bands resulted in relatively lower model accuracies at all maize growth stages (Table 4) in relation to VIs. For example, when estimating $EWT_{leaf}$, UAV bands exhibited the lowest accuracy at the V14-Vt and R1-R2 growth stages, yielding an RMSE of 47.58 $gm^{-2}$ and $R^2$ of 0.53, and RMSE of 13.13 $gm^{-2}$ and $R^2$ of 0.59, respectively. Similarly, in estimating maize $FMC_{leaf}$, the lowest RMSEs were obtained when using UAV bands at the R1-R2, R2-R3, and R3-R4 maize growth stage with RMSE of 1.13 $gm^{-2}$ and $R^2$ of 0.59, RMSE of 11.05 $gm^{-2}$, and $R^2$ of 0.53, and RMSE of 3.05 $gm^{-2}$ and $R^2$ of 0.57, respectively.

The use of VIs improved model accuracies of maize $EWT_{leaf}$ and $FMC_{leaf}$. For example, the $EWT_{leaf}$ model slightly improved by a magnitude of 6.43 from an RMSE of 47.58 to 41.15 $gm^{-2}$ at the V14-Vt maize growth stage. Again, in estimating $FMC_{leaf}$, using VIs improved the model accuracy from 11.05 to 7.94 $gm^{-2}$ at the R2-R3 growth stage.

### 3.2 Estimation of Maize $EWT_{leaf}$ Using the RF-Selected Spectral Variables Throughout the Stages

During the early vegetation growth stages, maize $EWT_{leaf}$ at the V8-V10 phenological stage was predicted to have an RMSE of 13.03 $gm^{-2}$ and $R^2$ of 0.69 (Fig. 5). The top-most influential predictor variables in estimating $EWT_{leaf}$ at this stage were $NDVI_{rededge}$, thermal, rededge,

**Table 4** Estimation accuracies of $EWT_{leaf}$ and $FMC_{leaf}$ derived using UAV bands in relation to the VIs.

| | | $EWT_{leaf}$ | | | $FMC_{leaf}$ | | |
|---|---|---|---|---|---|---|---|
| Maize growth stage | Predictor variables | $R^2$ | RMSE | rRMSE | $R^2$ | RMSE | rRMSE |
| **V8–V10** | UAV bands | 0.52 | 14.38 | 4.89 | 0.42 | 2.22 | 2.69 |
| | VIs | 0.6 | 14.98 | 4.91 | 0.44 | 2.35 | 2.85 |
| **V14–Vt** | UAV bands | 0.53 | 47.58 | 23.01 | 0.52 | 1.93 | 1.98 |
| | VIs | 0.7 | 41.15 | 19.9 | 0.56 | 2.15 | 2.76 |
| **R1–R2** | UAV bands | 0.59 | 13.13 | 6.46 | 0.59 | 1.13 | 1.34 |
| | VIs | 0.78 | 11.17 | 5.5 | 0.76 | 0.9 | 1.09 |
| **R2–R3** | UAV bands | 0.63 | 16.71 | 17.73 | 0.53 | 11.05 | 26.72 |
| | VIs | 0.7 | 37.21 | 50.67 | 0.73 | 7.94 | 18.71 |
| **R3–R4** | UAV bands | 0.58 | 24.49 | 18.71 | 0.57 | 3.05 | 4.47 |
| | VIs | 0.66 | 40.39 | 32.95 | 0.67 | 2.68 | 3.94 |

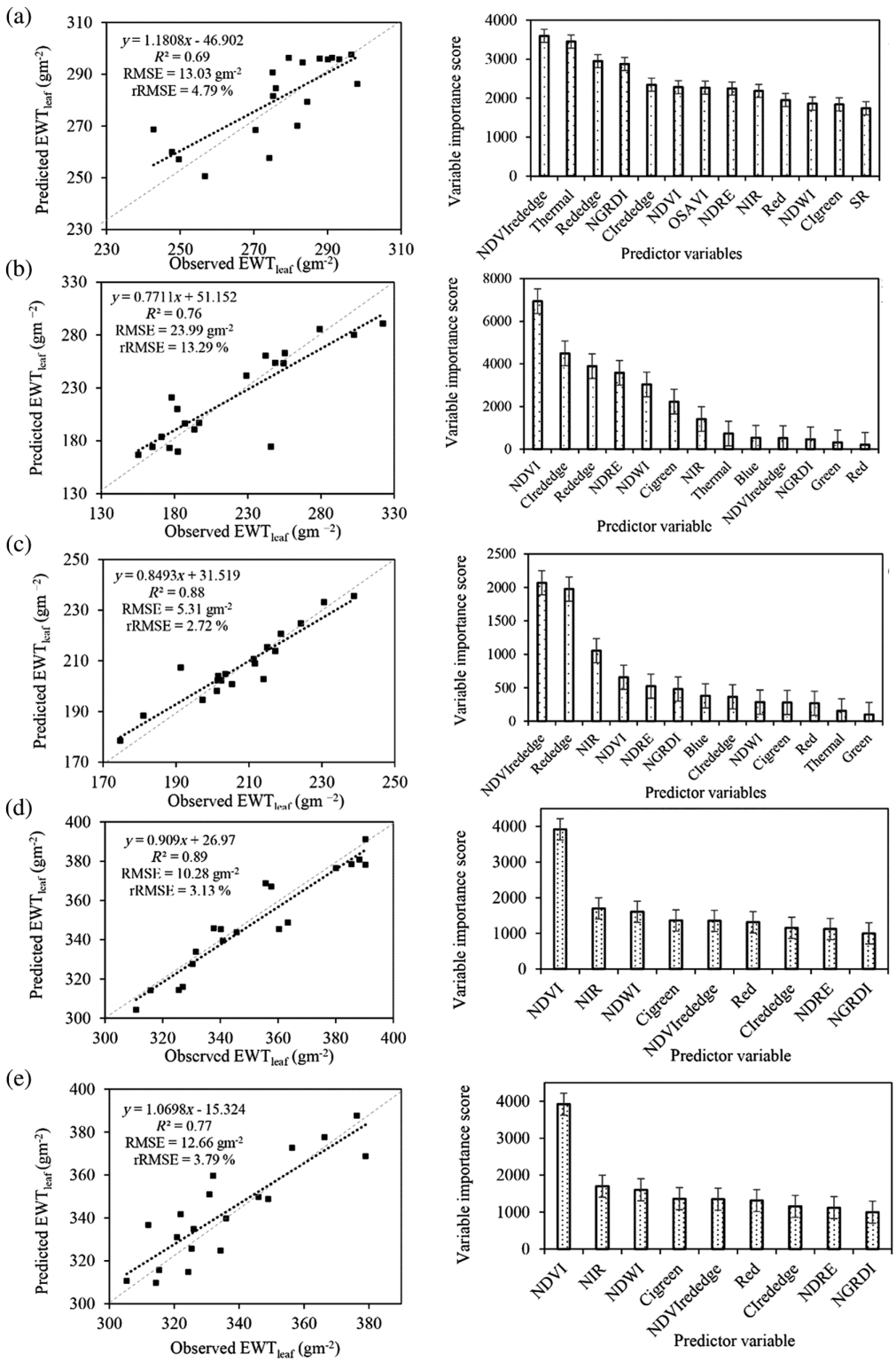


**Fig. 5** Relationship between the predicted and observed maize $EWT_{leaf}$ (right) and the variable importance scores (left) at (a) V8–V10, (b) V14–Vt, (c) R1–R2, (d) R2–R3, and (e) R3–R4 phenological growth stages and the model's variable importance scores of the optimal spectral predictors.

NGRDI, $CI_{rededge}$, NDVI, OSAVI, NDRE, NIR, red, NDWI, $CI_{green}$ and SR, in order of importance [Fig. 5(a)]. The V14-Vt exhibited the poorest prediction accuracy of maize $EWT_{leaf}$ during the vegetative stages (RMSE = 23.99 $gm^{-2}$ and $R^2$ of 0.76) using NDVI, $CI_{rededge}$, red-edge, NDRE, NDWI, $CI_{green}$, NIR, thermal, blue, $NDVI_{rededge}$, NGRDI, green, and red, in descending order of importance [Fig. 5(b)]. The most optimal maize growth stage for estimating $EWT_{leaf}$ was observed in the early reproductive R1-R2 growth stage, which yielded the highest model accuracy across all phenological stages (RMSE of 5.31 $gm^{-2}$ and $R^2$ of 0.88) based on $NDVI_{rededge}$, rededge, NIR, NDVI, NDRE, NGRDI, blue, $CI_{rededge}$, NDWI, and $CI_{green}$, red, thermal, and green, in order of importance [Fig. 5(c)]. Hereafter, a decrease in $EWT_{leaf}$ model accuracy was observed in all later stages of maize growth. For example, the estimation accuracy of $EWT_{leaf}$ decreased by 4.97 $gm^{-2}$ to an RMSE of 10.28 $gm^{-2}$ in the R2-R3 maize growth stage, compared to 5.31 $gm^{-2}$ from the R1-R2 stage. Nonetheless, an $R^2$ of 0.89 was attained from predicting maize $EWT_{leaf}$ during the R2-R3 growth stage. The influential predictor variables on that model included NDVI, NIR, NDWI, $CI_{green}$, $NDVI_{rededge}$, red, $CI_{rededge}$, NDRE, and NGRDI, accordingly [Fig. 5(d)]. Furthermore, the maize $EWT_{leaf}$ model accuracy depreciated at the R3-R4 growth stage yielding an RMSE of 12.66 $gm^{-2}$ and $R^2$ of 0.77. The influential spectral predictors from this model were NDVI, NIR, NDWI, $CI_{green}$, $NDVI_{rededge}$, and red, $CI_{rededge}$, NDRE, and NGRDI, in order of descending importance [Fig. 5(e)].

### 3.3 Estimation of Maize $FMC_{leaf}$ Using the RF-Selected Spectral Variables Throughout the Growing Stages

The estimation of maize $FMC_{leaf}$ at the V8-V10 growth stage yielded a moderate RMSE of 1.13%. However, it exhibited a low $R^2$ of 0.66 based on NDVI, $NDVI_{rededge}$, thermal, red, SR, rededge, NGRDI, green, NDWI, NIR, NDRE, OSAVI, $CI_{rededge}$, $CI_{green}$, and blue, in order of importance [Fig. 6(a)]. Meanwhile, at the V14-Vt growth stage, the estimation of maize $FMC_{leaf}$ yielded an RMSE = 1.44% and an optimal $R^2$ = 0.73. The most suitable predictor variables included NDRE, rededge, $CI_{green}$, NIR, NDWI, $CI_{rededge}$, NDVI, $NDVI_{rededge}$, thermal, green, blue, NGRDI, and red, in order of decreasing importance [Fig. 6(b)].

Meanwhile, the maize $FMC_{leaf}$ prediction accuracy significantly increased in the early reproductive stages of the maize growing stages. For example, the R1-R2 maize growth stage yielded an RMSE of 0.88% and an $R^2$ of 0.87 using NDVI, rededge, $NDVI_{rededge}$, NIR, NDRE, $CI_{rededge}$, blue, NGRDI, and red, in order of importance [Fig. 6(c)]. The optimal phenological growth stage for optimally estimating maize $FMC_{leaf}$ was the R2-R3 growth stage, which yielded the highest model accuracy with an RMSE = 0.45% and $R^2$ of 0.76. This optimal maize $FMC_{leaf}$ model was derived based on the NDRE, NIR, NDWI, $CI_{rededge}$, $NDVI_{rededge}$, rededge, $CI_{green}$, blue, thermal, NDVI, red, and green predictor variables [Fig. 6(d)].

Whereas the later reproductive growth stages demonstrated the lowest $FMC_{leaf}$ prediction accuracies. Maize $FMC_{leaf}$ at the R3-R4 growth stage yielded the poorest prediction accuracy with an RMSE of 1.54% and $R^2$ of 0.72. Finally, the most optimal variables that were selected in estimating maize $FMC_{leaf}$ at this growth stage were $NDVI_{rededge}$, $CI_{rededge}$, NDRE, NDWI, $CI_{green}$, NDVI, red, green, NIR, NGRDI, red-edge, thermal, and blue, in order of importance [Fig. 6(e)].

### 3.4 Comparing the Performance of Foliar Maize Moisture Content Indicators ($EWT_{leaf}$ and $FMC_{leaf}$) across the Growing Stages

When comparing the performance of $EWT_{leaf}$ and $FMC_{leaf}$, the results illustrate that the prediction accuracy of maize $EWT_{leaf}$ and $FMC_{leaf}$ varies for each phenological growth stage. For example, the maize $FMC_{leaf}$ outperformed $EWT_{leaf}$ with an rRMSE of 1.38% as opposed to an rRMSE of 4.79% [Figs. 5 and 6(a)]. Similarly, the prediction accuracy of maize $FMC_{leaf}$ (rRMSE = 1.88%) was significantly higher than that of maize $EWT_{leaf}$ (13.29%) by a magnitude of 11.41% [Figs. 5 and 6(b)]. Again, at the R1-R2 maize growth stage, $EWT_{leaf}$ exhibited an rRMSE of 2.72%, while $FMC_{leaf}$ of maize had a higher prediction accuracy with rRMSE of 1.08% [Figs. 5 and 6(c)]. Similarly, model accuracies for predicting maize $FMC_{leaf}$ were marginally higher than $EWT_{leaf}$ at the R2-R3 growth stage, with an rRMSE = 1% and 3.13%,

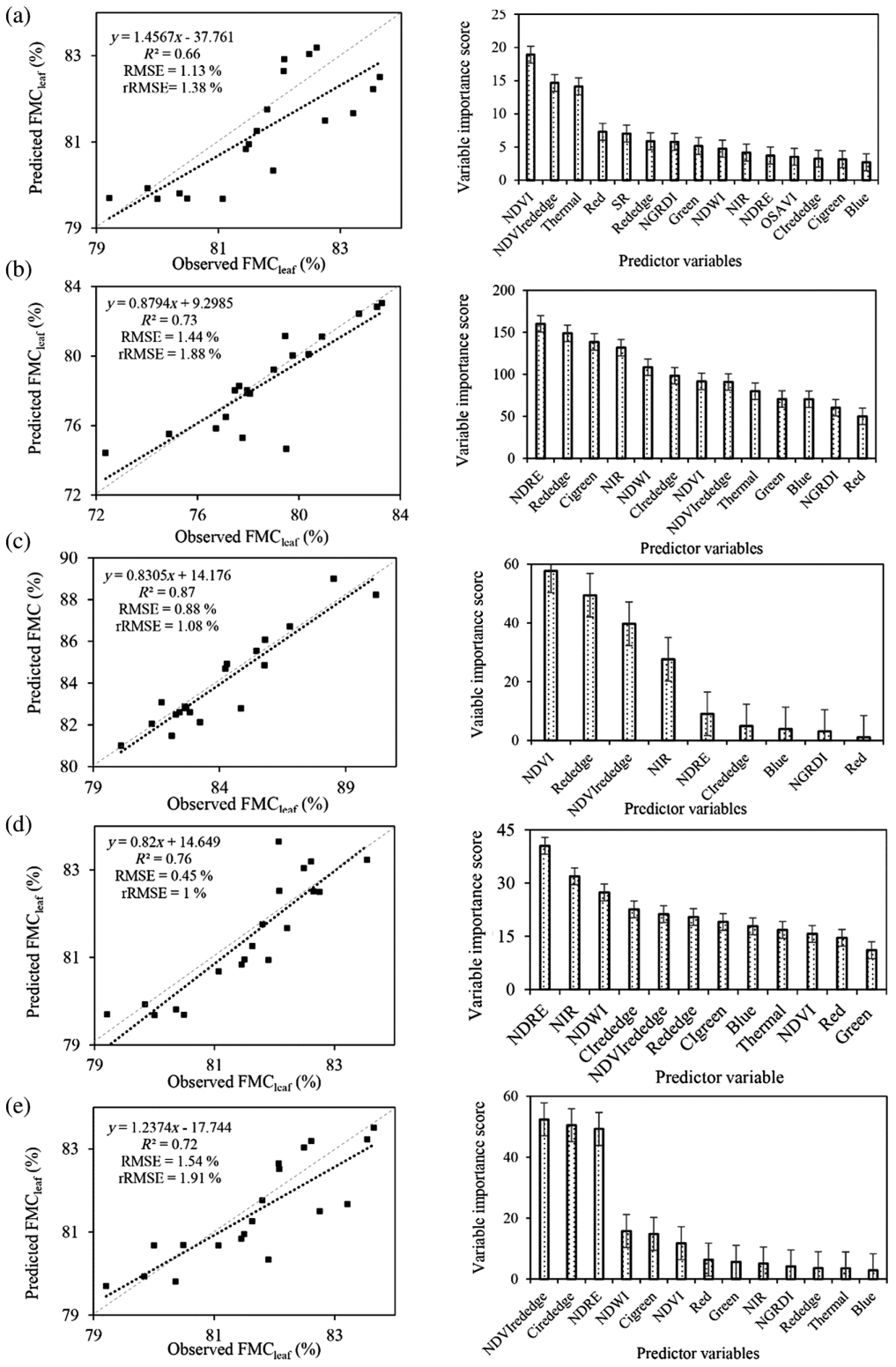


**Fig. 6** Relationship between the predicted and observed maize $FMC_{leaf}$ (right) and variable importance scores (left) at (a) V8–V10, (b) V14–Vt, (c) R1–R2, (d) R2–R3, and (e) R3–R4 phenological growth stages and the model's variable importance scores of the optimal spectral predictors.

respectively. Nonetheless, $EWT_{leaf}$ at this stage produced the highest $R^2$ of 0.89 compared to $FMC_{leaf}$, which yielded an $R^2$ of 0.76 [Figs. 5 and 6(d)]. Finally, $FMC_{leaf}$ produced an rRMSE of 1.91% at the R3-R4 maize growth stage, compared to the rRMSE of 3.79% exhibited by the maize $EWT_{leaf}$ model [Figs. 5 and 6(e)].

### 3.5 Spatial Variability of $EWT_{leaf}$ and $FMC_{leaf}$ across the Growing Stages

It was observed that maize $EWT_{leaf}$ and $FMC_{leaf}$ were higher in the eastern region and decreased toward the western section of the experimental maize plot (Figs. 7 and 8). The $EWT_{leaf}$ illustrated an increase in maize foliar moisture from the V8-V10 growth stage to the V14-Vt growth stage, where $EWT_{leaf}$ was at its highest. Thereafter, there was a slight decrease in maize foliar $EWT_{leaf}$

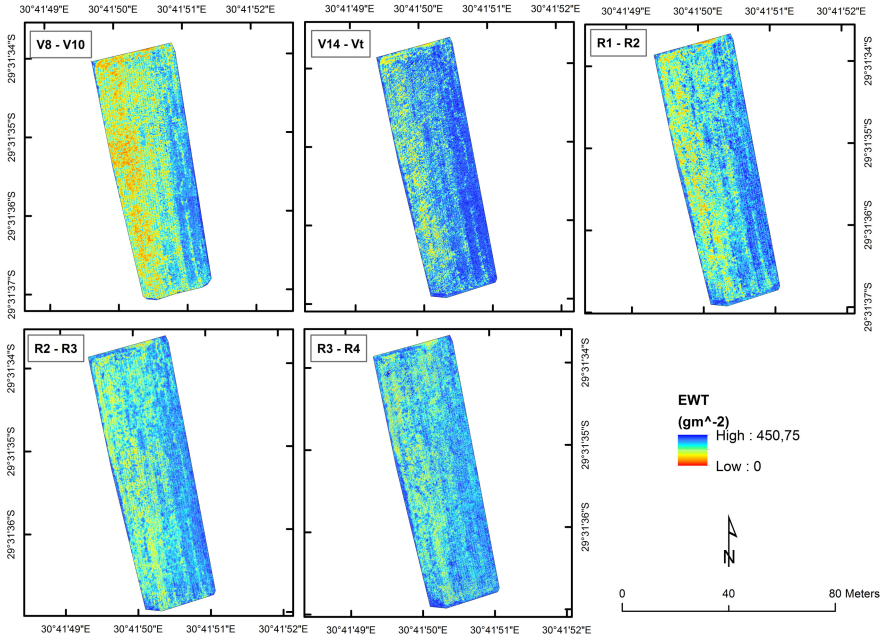


**Fig. 7** Spatial distribution of modeled maize $EWT_{leaf}$ across the growing stages.

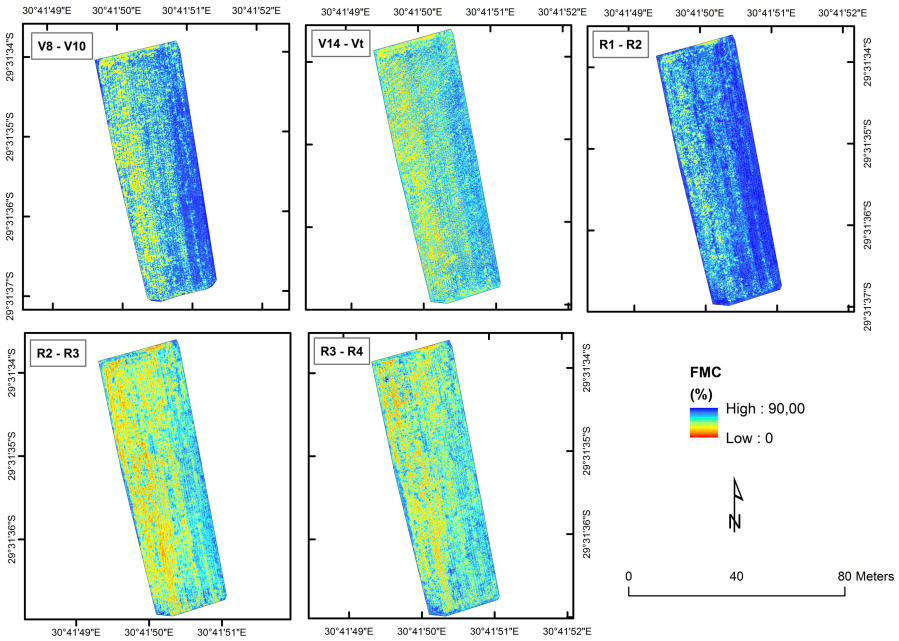


**Fig. 8** Spatial distribution of modeled maize $FMC_{leaf}$ across the growing stages.

in the early reproductive growth stage (R1-R2). However, the late reproductive stages (R2-R4) illustrated a lower $EWT_{leaf}$ yet a uniform distribution of maize foliar $EWT_{leaf}$ throughout the experimental plot (Fig. 7). Figure 8 demonstrated a high $FMC_{leaf}$ during the V8-V10 growth stage, followed by a significant decrease in $FMC_{leaf}$ during the V10-Vt growth stage. Thereafter, there was a progressive increase in maize foliar $FMC_{leaf}$ during the early reproductive stage (R1-R2). Subsequently, there was again a decrease in maize foliar $FMC_{leaf}$ during the late reproductive stages of maize (Fig. 8).

### 3.6 Descriptive Statistics and Temporal Variation in $EWT_{leaf}$ and $FMC_{leaf}$ during the Maize Growth Stages

As expected, there was a variation in maize $EWT_{leaf}$ and $FMC_{leaf}$ measured across the maize phenological stages (Fig. 9). Both maize $EWT_{leaf}$ and $FMC_{leaf}$ displayed a decreasing trend in moisture content as the growing stages progressed. The lowest mean $EWT_{leaf}$ were observed at the late reproductive stages of maize development, particularly during the R2-R3 stage ($96.45 \pm 62.15$ $gm^{-2}$), while the highest $EWT_{leaf}$ was at the V8-V10 growth stages ($274.45 \pm 43.25$ $gm^{-2}$) (Table 5). The R2-R3 growth stage had the lowest mean $FMC_{leaf}$ ($48.59 \pm 14.66\%$), while the greatest mean $FMC_{leaf}$ was observed at the R1-R2 maize growth stage ($84.48 \pm 2.23\%$) (Table 5). The results of a Kolmogorov–Smirnov normality test indicated

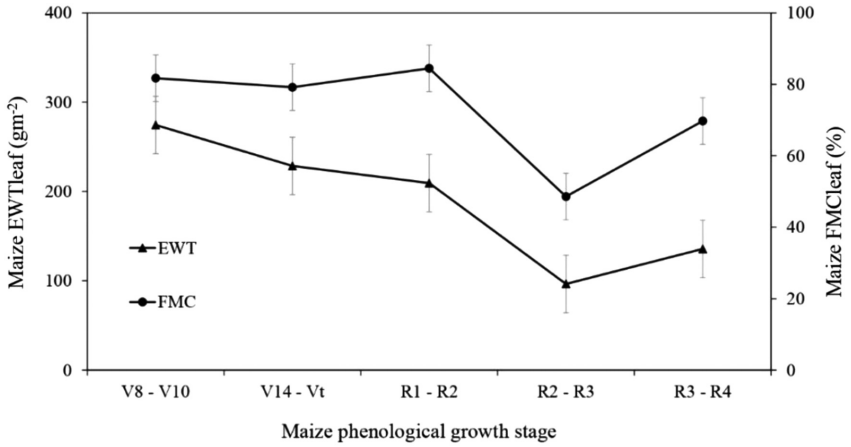


**Fig. 9** Temporal variation of maize $EWT_{leaf}$ and $FMC_{leaf}$ during the maize growing stages.

**Table 5** Descriptive statistics of $EWT_{leaf}$ and $FMC_{leaf}$ at the different phenological stages.

| Maize growth stage | Variable | Range (min-max) | Mean | Median | Std. | CV % | SEM |
|---|---|---|---|---|---|---|---|
| V8–V10 | EWT ($gm^{-2}$) | 169.35 to 462.73 | 274.45 | 270.47 | 43.25 | 15.76 | 5.45 |
| | FMC (%) | 73.72 to 90.91 | 81.72 | 81.63 | 2.32 | 2.84 | 0.29 |
| V14–Vt | EWT ($gm^{-2}$) | 154.76 to 329.33 | 228.57 | 229.13 | 49.67 | 21.73 | 6.26 |
| | FMC (%) | 69.93 to 86.05 | 79.17 | 79.01 | 2.89 | 3.65 | 0.36 |
| R1–R2 | EWT ($gm^{-2}$) | 159.86 to 249.66 | 209.38 | 211.34 | 17 | 8.12 | 2.14 |
| | FMC (%) | 77.78 to 91.59 | 84.48 | 84.23 | 2.73 | 3.24 | 0.34 |
| R2–R3 | EWT ($gm^{-2}$) | 11.66 to 448.71 | 9672.48 | 91.9 | 62.15 | 64.41 | 7.83 |
| | FMC (%) | 8.11 to 85.98 | 48.59 | 50 | 14.66 | 30.18 | 1.85 |
| R3–R4 | EWT ($gm^{-2}$) | 25.33 to 360.21 | 135.7 | 121.01 | 62.66 | 46.17 | 7.89 |
| | FMC (%) | 59.52 to 82.14 | 69.72 | 69.77 | 4.04 | 5.79 | 0.51 |

SEM is the standard error of mean, Std. is the standard deviation, and CV is the coefficient of variation.

that the distribution of the measured maize $EWT_{leaf}$ and $FMC_{leaf}$ did not significantly deviate from a normal distribution curve; hence a Pearson correlation was conducted to examine the relationship between maize $EWT_{leaf}$, $FMC_{leaf}$, and rainfall. Based on the Pearson correlation test, there was a statistically significant correlation between maize $EWT_{leaf}$ and rainfall ($R^2 = 0.97$, $p > 0.01$). Similarly, a correlation test between maize $FMC_{leaf}$ and rainfall indicated a statistically significant $R^2$ of 0.77 ($p > 0.01$).

## 4 Discussion

The emergence of UAV-derived data with high spatial and temporal resolutions presents a valuable tool for monitoring maize moisture content variability throughout the growing stages.[11] Reliable determination of spatio-temporal variations in maize moisture is necessary for the early detection of moisture stress and identification of moisture-sensitive growth stages, necessary for the development of precision agricultural management practices, especially at a farm scale.[4,30,64]

### 4.1 Estimation of Maize Foliar Moisture Indicators Using UAV-Derived Spectral Reflectance

Results of this study showed that optimal estimation of $EWT_{leaf}$ can be obtained between the silking–blister (R1-R2) growth stage of maize ($R^2 = 0.88$, RMSE = 5.31 $gm^{-2}$, and rRMSE = 2.72%) while for $FMC_{leaf}$ was the blister to milk (R2-R3) stage with an $R^2 = 0.76$ and RMSE = 0.45% (rRMSE = 1%) based on the red and NIR spectral variables. Literature confirms that the early reproductive growth stages are best suited for detecting physiological characteristics, such as leaf moisture content, using proximal remote sensing techniques.[65–67] This is because the transmittance spectra of the fully developed leaves and the canopy have minimal effects on the soil background and represent the maximum reflectance of leaf properties at that stage.[65,66] Furthermore, Prudnikova et al.[65] argued that estimating crop physiology at the early seedling and emergence vegetative growth stages is not optimum because sparse vegetation cover increases the interference of open soil surface reflectance, reducing prediction accuracy.

The findings of this study illustrate that VIs were the most optimal predictors of maize moisture content indicators compared to raw UAV-multispectral bands. These findings are not surprising since a large and growing body of literature has proven that the use of VIs derived from water-sensitive sections of the electromagnetic spectrum improves prediction accuracies and outperforms conventional bands in estimating crop moisture content indicators.[3,10,24,30,67]

The results in this study demonstrated that VIs derived from the NIR and rededge wavebands of the electromagnetic spectrum were the most sensitive spectral variable to maize foliar moisture indicators that RF selected. Specifically, the estimation of maize $EWT_{leaf}$ was greatly influenced by $NDVI_{rededge}$, rededge, NIR, and NDVI. The influence of NIR-based indices stems from the fact that this section of the electromagnetic spectrum is highly correlated to the quantity of water in leaf cells.[24] Literature confirms that the variation in leaf reflectance of turgid vegetation along the NIR wavelength, as a result of the changes in water transmissivity, and internal leaf structure, can be used to quantify crop moisture content and detect plants that are in a state of water deficit.[6,25] In addition, the sensitivity of the rededge band in maize moisture prediction can be explained by the fact that it is closely related to leaf chlorophyll composition, similar to the effect of nitrogen variation. When crops are experiencing moisture stress, as is the case with a decrease in plant nitrogen, there are declines in crop biological and physiochemical characteristics and processes, such as photosynthesis, foliar pigmentation, and leaf area, which are directly linked to leaf water status.[10,68] A reduction in moisture content results in the deceleration of the photosynthetic activity, which reduces the chlorophyll concentrations as the leaf halts its stomatal activities while losing turgidity and pigment.[30,69] These transitions are then detected from the red edge spectrum, which tends to shift toward the long-wavelength section.[3,10,67,70–72]

The impact of foliar moisture reduction and stress is spectrally similar to the impact of nitrogen reduction in terms of how they both impact photosynthesis, the foliar pigments and discoloration of the leaves, and overall plant productivity, which is sensitive to the rededge section of the electromagnetic spectrum.[73,74] This is not surprising because the macronutrient, $N$, is a solute taken in by plants from the soil as a solution in the solvent, water. Furthermore, both of them are major plant nutrition elements that are simultaneously required to optimize photosynthesis and

green pigment generation, which is then detected and monitored using the rededge and NIR spectrums widely proven in the literature.[73–75] This study's results agree with Liu et al.,[76] who found that the changes in the vegetation moisture content were spectrally discernible in the NIR spectral reflectance section. In a similar study, Zhang and Zhou[30] combined the NIR and rededge bands to form the NDRE, which became the most sensitive index to variations in maize moisture content ($R^2 = 0.75$). Furthermore, the results of this study concur with Sow et al.,[77] who used NDWI to predict vegetation FMC to an optimal accuracy of $R^2 = 0.85$.

Finally, the results of this study also revealed that chlorophyll-based indices, such as $CI_{green}$ and $CI_{rededge}$, were important predictors of maize foliar moisture content as they were among the most influential spectral variables on V14–Vt and R3–R4 stages when estimating maize $EWT_{leaf}$ and $FMC_{leaf}$. Again, this can be explained by the positive correlation between leaf chlorophyll content and water status, as prolonged moisture stress ultimately reduces chlorophyll pigmentation of maize leaves, thus changing leaf absorbance and reflectance characteristics.[3,67,69] In a similar study, Zhang et al.[67] concluded $CI_{green}$ and $CI_{rededge}$ are among the most influential predictors of maize EWT and FMC as they are highly sensitive to crop canopy water variation. Despite the apparent limitations of NDVI, as stated in the literature,[28,78] this index was an important predictor of maize moisture indicators in this study. This is explained by the fact that the NDVI is an effective indicator of leaf photosynthetic capacity, which is correlated to leaf greenness and water status.[3,26]

The results of this study concur with those of Wang et al.[64] They successfully used NDVI to monitor maize water variability using a seasonal NDVI time series analysis. Easterday et al.[68] noted that the NDVI could discriminate variations in vegetation moisture stress and accurately predict leaf water content to an $R^2$ of 0.89. In addition, it was observed that there was significant variability in the importance scores of the predictor variables across the growing season (Figs. 6 and 7). This could be attributed to the variations in the interaction between the incident energy and the maize crop biochemical and physical variations as a function of moisture variability at different growth stages. Moisture regulates plant productivity and biomass accumulation. The leave and accumulated biomass interact differently with different sections of the electromagnetic spectrum facilitating the variation in the most optimal spectral features selected as well as the magnitude of their influence in various models. As aforementioned, most of these selected optimal spectral features (Figs. 5 and 7) were derived from the NIR and rededge spectrums.

### 4.2 Comparison of $EWT_{leaf}$ and $FMC_{leaf}$ as Indicators of Maize Foliar Moisture Content

The findings of this study illustrate that maize foliar $EWT_{leaf}$ and $FMC_{leaf}$ vary at each phenological stage across the growing stages. The variations between these two maize foliar moisture indicators can be explained by the fact that $EWT_{leaf}$ quantifies moisture content as a function of leaf area and $FMC_{leaf}$ computes moisture content as the proportion of water to dry matter.[8,79] Literature confirms that leaf area is an essential characteristic of moisture content, as a decrease in leaf area could indicate crop moisture stress.[79,80] This is because there is a leaf transpiration reduction when crops are moisture stressed, as crops reduce their leaf area to sustain moisture levels.[67,81] Furthermore, the variations in $EWT_{leaf}$ and $FMC_{leaf}$ models can be explained by the relationship between crop health and moisture content.[30] The variability of crop moisture content is largely influenced by crop health, which affects leaf physiochemical characteristics that will, as a result, reflect differently along various spectral regions of the electromagnetic spectrum.[6,9,24]

UAVs are fast becoming a key component of precision agriculture as they provide opportunities for mainstreaming climate-smart agricultural practices into smallholder farming systems for improved crop health monitoring and water resource management. Understanding the spatio-temporal variation in maize moisture can support smallholder agricultural decision-making to facilitate the development of crop-specific management plans to increase production and resilience while reducing the susceptibility of these resources stricken cropping systems to future impacts of climate variability. Specifically, information on foliar moisture variability could inform farmers of the need to supplement rainfed systems with irrigation water to optimize crop production. Furthermore, the methods used in this study could be adapted to monitor other crops' moisture content within smallholder farming systems. Future studies should assess maize

moisture variability across various climates and evaluate the influence of other agronomical factors, such as soil structure and topographic effects, on leaf moisture status.

## 5 Conclusion

This study sought to test the utility of UAV-based multispectral data in estimating leaf EWT and FMC of smallholder maize crops across the growing stages. The results showed that the UAV-derived multispectral data could be useful in quantifying maize moisture variability at a high spatial and temporal resolution. Therefore, it can be concluded that:

- UAV-derived multispectral data can optimally characterize maize EWT ($R^2 = 0.88$, RMSE $= 5.31$ gm$^{-2}$, and rRMSE $= 2.72\%$) and FMC ($R^2 = 0.76$, RMSE $= 0.45\%$, and rRMSE $= 1\%$) variations using spectral variables from the NIR and red-edge wavelengths of the electromagnetic spectrum, which demonstrated great sensitivity to the variation in maize moisture content;
- The phases between silking and milk reproductive growth stage are the most optimal growth stages for predicting maize moisture content using UAV-derived data.

This study demonstrates the potential of UAV-based proximal remote sensing techniques in providing near-real-time and spatially explicit information on maize moisture variability across the growing stages. Finally, this study will allow for optimizing marginalized communities' agricultural productivity to improve their livelihoods in light of climate change, thus enhancing food and nutrition security.

### Disclosures

The authors declare no potential conflicts of interest to disclose.

### Code and Data Availability

The data that support the findings of this article are not publicly available due to authorization restrictions from the funder that limit the distribution of data as the article is part of an ongoing project where other manuscripts are still being prepared. They can be requested from the author at 216016417@stu.ukzn.ac.za upon project completion.

### Acknowledgments

The authors would like to recognize the support of the Centre for Transformative Agricultural and Food Systems through the uMngeni Resilience Project, which is funded by the Adaptation Fund. The authors also wish to thank Dr. Trylee Matongera, Siphiwokuhle Buthelezi, Kiara Brewer, Israel Odebiri, Serge Kiala, Welcome Ngcobo, and Amanda Nyawose for their assistance with fieldwork and laboratory logistics. Additionally, the authors extend their gratitude to the 2023 Asian Conference on Remote Sensing, for providing a platform to present the findings of this research. The authors specifically acknowledge the proceedings paper titled "Drone-derived multispectral data for the derivation of maize leaf equivalent water thickness and fuel moisture content in smallholder maize farming."

### References

1. T. Ge et al., "Effects of water stress on growth, biomass partitioning, and water-use efficiency in summer maize (*Zea mays L.*) throughout the growth cycle," *Acta Physiologiae Plantarum* **34**(3), 1043–1053 (2012).
2. R. Sah et al., "Impact of water deficit stress in maize: phenology and yield components," *Sci. Rep.* **10**(1), 2944 (2020).
3. H. S. Ndlovu et al., "A comparative estimation of maize leaf water content using machine learning techniques and unmanned aerial vehicle (UAV)-based proximal and remotely sensed data," *Remote Sens.* **13**(20), 4091 (2021).
4. F. Ghooshchi, M. Seilsepour, and P. Jafari, "Effects of water stress on yield and some agronomic traits of maize (SC 301)," *Am. Eurasian J. Agric. Environ. Sci.* **4**(3), 302–305 (2008).
5. U. Ray et al., "Morpho-phenological and yield responses of maize (*Zea mays* L.) to non-irrigated water stress condition," *J. Sci. Technol.* **8**, 15 (2020).

6. M. R. Mobasheri and S. B. Fatemi, "Leaf equivalent water thickness assessment using reflectance at optimum wavelengths," *Theor. Exp. Plant Physiol.* **25**(3), 196–202 (2013).
7. Q. Yi et al., "Leaf and canopy water content estimation in cotton using hyperspectral indices and radiative transfer models," *Int. J. Appl. Earth Observ. Geoinf.* **33**, 67–75 (2014).
8. A. Elsherif, R. Gaulton, and J. Mills, "Measuring leaf equivalent water thickness of short-rotation coppice willow canopy using terrestrial laser scanning," in *IGARSS 2019-2019 IEEE Int. Geosci. and Remote Sens. Symp.* (2019).
9. F. Zhang and G. Zhang, "Estimation of vegetation water content using hyperspectral vegetation indices: a comparison of crop water indicators in response to water stress treatments for summer maize," *BMC Ecol.* **19**(1), 18 (2019).
10. M. Sibanda et al., "Quantitative assessment of grassland foliar moisture parameters as an inference on rangeland condition in the mesic rangelands of southern Africa," *Int. J. Remote Sens.* **42**(4), 1474–1491 (2021).
11. W. Chivasa, O. Mutanga, and C. Biradar, "UAV-based multispectral phenotyping for disease resistance to accelerate crop improvement under changing climate conditions," *Remote Sens.* **12**(15), 2445 (2020).
12. L. Zhang et al., "Monitoring the leaf water content and specific leaf weight of cotton (*Gossypium hirsutum* L.) in saline soil using leaf spectral reflectance," *Eur. J. Agron.* **41**, 103–117 (2012).
13. X. Jin et al., "Determination of leaf water content by visible and near-infrared spectrometry and multivariate calibration in *Miscanthus*," *Front. Plant Sci.* **8**, 721 (2017).
14. J. Yue et al., "A comparison of crop parameters estimation using images from UAV-mounted snapshot hyperspectral sensor and high-definition digital camera," *Remote Sens.* **10**(7), 1138 (2018).
15. W. H. Maes and K. Steppe, "Perspectives for remote sensing with unmanned aerial vehicles in precision agriculture," *Trends Plant Sci.* **24**(2), 152–164 (2019).
16. H. Hoffmann et al., "Crop water stress maps for an entire growing season from visible and thermal UAV imagery," *Biogeosciences* **13**(24), 6545–6563 (2016).
17. J. Tang, W. Han, and L. Zhang, "UAV multispectral imagery combined with the FAO-56 dual approach for maize evapotranspiration mapping in the North China plain," *Remote Sens.* **11**(21), 2519 (2019).
18. J. Everaerts, "The use of unmanned aerial vehicles (UAVs) for remote sensing and mapping," *Int. Arch. Photogramm. Remote Sens. Sp. Inf. Sci.* **37**, 1187–1192 (2008).
19. Y. Guo et al., "Machine learning-based approaches for predicting SPAD values of maize using multi-spectral images," *Remote Sens.* **14**(6), 1337 (2022).
20. G. Pajares, "Overview and current status of remote sensing applications based on unmanned aerial vehicles (UAVs)," *Photogramm. Eng. Remote Sens.* **81**(4), 281–330 (2015).
21. D. C. Tsouros, S. Bibi, and P. G. Sarigiannidis, "A review on UAV-based applications for precision agriculture," *Information* **10**(11), 349 (2019).
22. A.-V. Emilien, C. Thomas, and H. Thomas, "UAV & satellite synergies for optical remote sensing applications: a literature review," *Sci. Remote Sens.* **3**, 100019 (2021).
23. A. Matese et al., "Intercomparison of UAV, aircraft and satellite remote sensing platforms for precision viticulture," *Remote Sens.* **7**(3), 2971–2990 (2015).
24. N. Pasqualotto et al., "Retrieval of canopy water content of different crop types with two new hyperspectral indices: water absorption area index and depth water index," *Int. J. Appl. Earth Observ. Geoinf.* **67**, 69–78 (2018).
25. A. Chemura, O. Mutanga, and T. Dube, "Remote sensing leaf water stress in coffee (*Coffea arabica*) using secondary effects of water absorption and random forests," *Phys. Chem. Earth Parts A/B/C* **100**, 317–324 (2017).
26. C. Wijewardana et al., "Physiological assessment of water deficit in soybean using midday leaf water potential and spectral features," *J. Plant Interactions* **14**(1), 533–543 (2019).
27. G. Krishna et al., "Comparison of various modelling approaches for water deficit stress monitoring in rice crop through hyperspectral remote sensing," *Agric. Water Manage.* **213**, 231–244 (2019).
28. J. Xue and B. Su, "Significant remote sensing vegetation indices: a review of developments and applications," *J. Sens.* **2017**, 1353691 (2017).
29. C. Xu et al., "Monitoring crop water content for corn and soybean fields through data fusion of MODIS and Landsat measurements in Iowa," *Agric. Water Manage.* **227**, 105844 (2020).
30. F. Zhang and G. Zhou, "Estimation of canopy water content by means of hyperspectral indices based on drought stress gradient experiments of maize in the north plain China," *Remote Sens.* **7**(11), 15203–15223 (2015).
31. R. Latif, A. Saddik, and A. Elouardi, "Evaluation of agricultural precision algorithms on UAV images," in *Int. Conf. Comput. Sci. and Renew. Energies (ICCSRE)* (2019).
32. I. J. Miller et al., "Analyzing crop health in vineyards through a multispectral imaging and drone system," in *Syst. and Inf. Eng. Des. Symp. (SIEDS)* (2020).
33. Y. Guo et al., "Integrated phenology and climate in rice yields prediction using machine learning methods," *Ecol. Indicators* **120**, 106935 (2021).

34. Y. Guan et al., "Prediction of soil water content and electrical conductivity using random forest methods with UAV multispectral and ground-coupled geophysical data," *Remote Sens.* **14**(4), 1023 (2022).
35. N. Horning, "Random forests: an algorithm for image classification and generation of continuous fields data sets," in *Proc. Int. Conf. Geoinf. for Sp. Infrastruct. Dev. in Earth and Allied Sci.*, Osaka, Japan (2010).
36. Q. Guo et al., "Urban tree classification based on object-oriented approach and random forest algorithm using unmanned aerial vehicle (UAV) multispectral imagery," *Remote Sens.* **14**(16), 3885 (2022).
37. G. Shao et al., "Mapping maize crop coefficient Kc using random forest algorithm based on leaf area index and UAV-based multispectral vegetation indices," *Agric. Water Manage.* **252**, 106906 (2021).
38. Q. Feng, J. Liu, and J. Gong, "UAV remote sensing for urban vegetation mapping using random forest and texture analysis," *Remote Sens.* **7**(1), 1074–1094 (2015).
39. E. B. Henderson, D. M. Bell, and M. J. Gregory, "Vegetation mapping to support greater sage-grouse habitat monitoring and management: multi-or univariate approach?" *Ecosphere* **10**(8), e02838 (2019).
40. H. Lee, J. Wang, and B. Leblon, "Using linear regression, random forests, and support vector machine with unmanned aerial vehicle multispectral images to predict canopy nitrogen weight in corn," *Remote Sens.* **12**(13), 2071 (2020).
41. K. Brewer et al., "Predicting the chlorophyll content of maize over phenotyping as a proxy for crop health in smallholder farming systems," *Remote Sens.* **14**(3), 518 (2022).
42. S. Keen and H. Winkler, "Enhanced direct access finance in South Africa: SANBI and the adaptation fund," University of Cape Town, http://tinyurl.com/5ssrdv95 (2020).
43. K. Shen et al., "Crop area estimation from UAV transect and MSR image data using spatial sampling method," *Proc. Environ. Sci.* **26**, 95–100 (2015).
44. G. A. Wood, J. C. Taylor, and R. J. Godwin, "Calibration methodology for mapping within-field crop variability using remote sensing," *Biosyst. Eng.* **84**(4), 409–423 (2003).
45. D. J. Mulla, "Twenty five years of remote sensing in precision agriculture: key advances and remaining knowledge gaps," *Biosyst. Eng.* **114**(4), 358–371 (2013).
46. X. Zhao et al., "Functional mapping of ontogeny in flowering plants," *Brief. Bioinform.* **13**(3), 317–328 (2012).
47. A. Wahbi and W. Avery, "*In situ* destructive sampling," in *Cosmic Ray Neutron Sensing: Estimation of Agricultural Crop Biomass Water Equivalent*, pp. 5–9, Springer, Cham (2018).
48. N. Sade, E. Galkin, and M. Moshelion, "Measuring arabidopsis, tomato and barley leaf relative water content (RWC)," *Bio-protocol* **5**(8), 1451 (2015).
49. M. Cubero-Castan et al., "Assessment of the radiometric accuracy in a target less work flow using Pix4D software," in *9th Workshop on Hyperspectral Image and Signal Process.: Evol. in Remote Sens. (WHISPERS)* (2018).
50. B.-C. Gao, "NDWI: a normalized difference water index for remote sensing of vegetation liquid water from space," *Remote Sens. Environ.* **58**(3), 257–266 (1996).
51. J. Rouse et al., "Monitoring vegetation systems in the great plains with ERTS," in *Proc. 3rd ERTS Symp.*, Washington, DC (1974).
52. P. J. Zarco-Tejada et al., "Scaling-up and model inversion methods with narrowband optical indices for chlorophyll content estimation in closed forest canopies with hyperspectral data," *IEEE Trans. Geosci. Remote Sens.* **39**(7), 1491–1507 (2001).
53. A. Gitelson and M. N. Merzlyak, "Spectral reflectance changes associated with autumn senescence of *Aesculus hippocastanum L.* and *Acer platanoides L.* leaves. Spectral features and relation to chlorophyll estimation," *J. Plant Physiol.* **143**(3), 286–292 (1994).
54. A. A. Gitelson, Y. Gritz, and M. N. Merzlyak, "Relationships between leaf chlorophyll content and spectral reflectance and algorithms for non-destructive chlorophyll assessment in higher plant leaves," *J. Plant Physiol.* **160**(3), 271–282 (2003).
55. C. F. Jordan, "Derivation of leaf-area index from quality of light on the forest floor," *Ecology* **50**(4), 663–666 (1969).
56. X.-L. Jin et al., "Estimation of wheat agronomic parameters using new spectral indices," *PLoS One* **8**(8), e72736 (2013).
57. B. Lu and Y. He, "Evaluating empirical regression, machine learning, and radiative transfer modelling for estimating vegetation chlorophyll content using bi-seasonal hyperspectral images," *Remote Sens.* **11**(17), 1979 (2019).
58. J. H. Jeong et al., "Random forests for global and regional crop yield predictions," *PLoS One* **11**(6), e0156571 (2016).
59. E. M. Abdel-Rahman, F. B. Ahmed, and R. Ismail, "Random forest regression and spectral band selection for estimating sugarcane leaf nitrogen concentration using EO-1 Hyperion hyperspectral data," *Int. J. Remote Sens.* **34**(2), 712–728 (2013).
60. W. Chivasa, O. Mutanga, and J. Burgueño, "UAV-based high-throughput phenotyping to increase prediction and selection accuracy in maize varieties under artificial MSV inoculation," *Comput. Electron. Agric.* **184**, 106128 (2021).

61. S. Adelabu et al., "Exploiting machine learning algorithms for tree species classification in a semiarid woodland using RapidEye image," *J. Appl. Remote Sens.* **7**(1), 073480 (2013).
62. L. Breiman, "Random forests," *Mach. Learn.* **45**(1), 5–32 (2001).
63. A. M. Prasad, L. R. Iverson, and A. Liaw, "Newer classification and regression tree techniques: bagging and random forests for ecological prediction," *Ecosystems* **9**(2), 181–199 (2006).
64. R. Wang, K. Cherkauer, and L. Bowling, "Corn response to climate stress detected with satellite-based NDVI time series," *Remote Sens.* **8**(4), 269 (2016).
65. E. Prudnikova et al., "Influence of soil background on spectral reflectance of winter wheat crop canopy," *Remote Sens.* **11**(16), 1932 (2019).
66. C. S. Daughtry et al., "Estimating corn leaf chlorophyll concentration from leaf and canopy reflectance," *Remote Sens. Environ.* **74**(2), 229–239 (2000).
67. L. Zhang et al., "Mapping maize water stress based on UAV multispectral remote sensing," *Remote Sens.* **11**(6), 605 (2019).
68. K. Easterday et al., "Remotely sensed water limitation in vegetation: insights from an experiment with unmanned aerial vehicles (UAVs)," *Remote Sens.* **11**(16), 1853 (2019).
69. S. Liu et al., "Remote estimation of leaf and canopy water content in winter wheat with different vertical distribution of water-related properties," *Remote Sens.* **7**(4), 4626–4650 (2015).
70. G. A. Carter, "Responses of leaf spectral reflectance to plant stress," *Am. J. Botany* **80**(3), 239–243 (1993).
71. C. Ballester et al., "Monitoring the effects of water stress in cotton using the green red vegetation index and red edge ratio," *Remote Sens.* **11**(7), 873 (2019).
72. K. Brewer et al., "Estimation of maize foliar temperature and stomatal conductance as indicators of water stress based on optical and thermal imagery acquired using an unmanned aerial vehicle (UAV) platform," *Drones* **6**(7), 169 (2022).
73. D. El-Shikha et al., "Ground-based remote sensing for assessing water and nitrogen status of broccoli," *Agric. Water Manage.* **92**(3), 183–193 (2007).
74. D. Clay et al., "Characterizing water and nitrogen stress in corn using remote sensing," *Agron. J.* **98**(3), 579–587 (2006).
75. A. K. Tilling et al., "Remote sensing of nitrogen and water stress in wheat," *Field Crops Res.* **104**(1–3), 77–85 (2007).
76. L. Liu, S. Zhang, and B. Zhang, "Evaluation of hyperspectral indices for retrieval of canopy equivalent water thickness and gravimetric water content," *Int. J. Remote Sens.* **37**(14), 3384–3399 (2016).
77. M. Sow et al., "Estimation of herbaceous fuel moisture content using vegetation indices and land surface temperature from MODIS data," *Remote Sens.* **5**(6), 2617–2638 (2013).
78. T. J. Jackson et al., "Vegetation water content mapping using Landsat data derived normalized difference water index for corn and soybeans," *Remote Sens. Environ.* **92**(4), 475–482 (2004).
79. C. Zhang et al., "Capability of crop water content for revealing variability of winter wheat grain yield and soil moisture under limited irrigation," *Sci. Tot. Environ.* **631**, 677–687 (2018).
80. L. Song, J. Jin, and J. He, "Effects of severe water stress on maize growth processes in the field," *Sustainability* **11**(18), 5086 (2019).
81. M. García et al., "Combining AVHRR and meteorological data for estimating live fuel moisture content," *Remote Sens. Environ.* **112**(9), 3618–3627 (2008).


**Helen S. Ndlovu** is a doctoral candidate in environmental science at the University of KwaZulu-Natal. With a solid foundation in environmental management, biology, and remote sensing and geographic information systems, her research centers on leveraging unmanned aerial vehicle technology and multispectral-thermal data for agricultural monitoring, particularly in addressing challenges faced by smallholder farming systems. Her expertise extends to previous research endeavors in rangeland management and the mapping of alien invasive plant distributions, showcasing her commitment to advancing both sustainable agriculture and environmental conservation.

Biographies of the other authors are not available.